



ARCHIVES
of
FOUNDRY ENGINEERING

ISSN (2299-2944)
Volume 2023
Issue 4/2023

145 – 156

17/4

10.24425/afe.2023.146689

Published quarterly as the organ of the Foundry Commission of the Polish Academy of Sciences



The Influence of Pearlite Present in the Microstructure of GX120MnCr13 Cast Steel on Wear Resistance

B. Kalandyk ^{a,*} , R.E. Zapala ^a , I. Sulima ^b , P. Furmańczyk ^c , J. Kasińska ^c 

^a AGH University of Krakow, Faculty of Foundry Engineering,
al. A. Mickiewicza 30, 30-059 Krakow, Poland

^b University of the National Education Commission Krakow, Institute of Technology,
ul. Podchorążych 2, 32-084 Krakow, Poland

^c Kielce University of Technology, Faculty of Mechatronics and Mechanical Engineering, Poland

* Corresponding author: E-mail address: bk@agh.edu.pl

Received 02.11.2023; accepted in revised form 03.12.2023; available online 29.12.2023

Abstract

The article presents the results of metallographic and tribological tests on GX120MnCr13 cast steel that was previously subjected to heat treatment (including solution treatment from 1100°C and isothermal holding at 250, 400, and 600°C for 100 hours). The temperatures of the isothermal holding process were selected in order to reflect the possible working conditions of the cast elements that can be made of this cast steel. Wear tests were carried out under dry friction conditions using the ball-on-disc method using a ZrO₂ ball as a counter-sample. The tests were carried out with a load of 5 N. The influence of the long-term isothermal holding process on the microstructure of the tested cast steel was analysed by light and scanning microscopy; however, abrasion marks were also examined using a confocal microscope. Based on the tests conducted, it was found that in the microstructures of the sample after solution treatment and samples that were held in isothermal condition at 250 and 400°C, the grain boundary areas were enriched in Mn and Cr compared to the areas inside the grains. Pearlite appeared in the sample that was heated (or held in isothermal holding) at 600°C; its share reached 41.6%. The presence of pearlite in the austenitic matrix increased the hardness to 351.4 HV₁₀. The hardness of the remaining tested samples was within a range of 221.8–229.1 HV₁₀. Increasing the hardness of the tested cast steel directly resulted in a reduction in the degree of wear as well as the volume, area, and width of the abrasion marks. A microscopic analysis of the wear marks showed that the dominant process of the abrasive wear of the tested friction pair was the detachment and displacement of the tested material through the indentation as a result of the cyclical impact of the counter-sample.

Keywords: Hadfield cast steel, Microstructure, Hardness, Ball-on-disc test, Wear resistance

1. Introduction

High-manganese cast steel that contains 1.0% C and about 13% Mn (also called Hadfield cast steel) belongs to the group of wear-resistant materials [1–3]. This is a material that is particularly

appreciated in the mining and power industries (e.g. elements of coal mills) [3, 4] as well as railways [5, 6]; i.e. where there are difficult working conditions. This results primarily from the complexity of the phenomena that occur during the wear and cause the plastic deformation of the cooperating surfaces of cast



© The Author(s) 2023. Open Access. This article is licensed under a Creative Commons Attribution 4.0 International License (<http://creativecommons.org/licenses/by/4.0/>), which permits use, sharing, adaptation, distribution and reproduction in any medium or format, as long as you give appropriate credit to the original author(s) and the source, provide a link to the Creative Commons licence, and indicate if changes were made.

elements. In [7], it was pointed out that, when testing the abrasive wear of Hadfield steel that works in an aqueous abrasive environment, even the pH value of the abrasive solution and the size of the abrasive particles should be taken into account.

An inseparable phenomenon that occurs during the operation of cast elements are changes in the structure of the material itself that are related to temperature changes during the operation of elements that are made of this cast steel, for example [2]. Such an effect can be seen in impact crushers at high hammer speeds. As a result of increasing the temperature of the material during the operation of the hammers, the appearance of acicular precipitates of manganese cementite and their accelerated cracking may occur [8, 9]. At a temperature of about 550°C, pearlite may be formed after one hour; this can reach up to 22% of the structure, reducing the ductility and increasing the brittleness of Hadfield steel [10]. According to Martin et al., the beginning of the diffusion transformation of the pearlite begins at temperatures of above 450°C and depends on the time of the isothermal holding [10]. At first, the pearlite begins to form on the grain boundaries and, later, in the forms of islands inside them. At the same time, the austenitic matrix is depleted of its C and Mn [11]. With a lamellar structure/morphology, the manganese cementite (Fe, Mn)₃C that is present in the pearlite increases the hardness and brittleness of the pearlite areas as compared to the austenitic matrix. In turn, this reduces the properties of Hadfield steel. According to research [11], a 20–30% share of pearlite in the Hadfield steel structure is responsible for significant reductions in elongation, contraction, and tensile strength. The cementite that can be observed in high-manganese cast steels with the addition of Cr is additionally enriched in Cr, which contributes to the increase in the hardness of the cast steel [12].

Many publications [13, 14] have drawn attention to the role of the chemical composition and modification of Hadfield steel and cast steel on their properties. This has been the direction of the research of many research centres, because the type and morphology of the carbides that are produced in the matrix can improve the wear resistance. The basic elements that are introduced into high-manganese cast steel in order to produce primary carbides are Ti [15–17], V [18], or Nb [19].

The wear rate of Hadfield steel at various loads within a range of 2.5–15 N and the change in the content of C and Mn were the subjects of research by Gürol et al. [20]. They pointed out the decrease in the rate of wear with the increase in the contents of these elements (but only at loads of up to 10 N). When the load was increased to 15 N, there was a sharp increase in the wear rate due to the additional presence of particles that formed during the test. The authors of the paper [21] came to similar conclusions; they noticed that increasing the Mn content to 18% and adding Cr (2.3%) contributed to an increase in wear resistance under dry friction conditions (with a load of 10 N) when compared to the classic GX120Mn13 cast steel. It is well-known that the rate of wear mainly depends on two factors: the microstructure, and the hardness of the alloy [22, 23]. In the case of Hadfield cast steel, changes in its microstructure and hardness are also caused by its earlier hardening (which reduces the wear later) [24]. Interesting results regarding wear resistance were presented by the authors of [25]; they found that introducing Mg into Hadfield steel in its as-cast state reduces the wear rate by up to 300% as compared to conventional heat treated material. Their results confirmed that the

amount of wear depends on the morphology of the phases that are present in the alloy. However, the presented results did not show the impact of the hardness on wear resistance.

The aim of the research that was conducted by the authors of this paper was to demonstrate the influence of the microstructure of GX120MnCr13 cast steel castings that were obtained during isothermal holdings at 250, 400, and 600°C for 100 hours on its wear. The isothermal holding temperatures were selected in such a way that they corresponded to the range of extreme operating temperatures of castings that are made of this cast steel. In addition, isothermal holding was carried out at a temperature of 600°C (at which pearlite is present in the austenitic matrix according to thermodynamic calculations). In the tests, a holding time of 100 hours was assumed to obtain the maximum possible amount of the pearlitic phase in each instance. The authors assumed that the presence of evenly distributed pearlite islands in the austenitic matrix could increase the resistance to abrasive wear under a load of 5 N.

2. Materials and methods

High-manganese GX120MnCr13 cast steel that was melted in a laboratory induction electric furnace was used for this study. The charge for melting was composed of manganese and carbon cast steel scrap and ferroalloys, which were used to supplement the chemical composition. Al and Ca-Si were used for deoxidation; then, the bath was modified with Fe-Ti. The analysis of the chemical composition of the melted alloy was performed using the Foundry-Master spark spectrometer by Oxford Instruments Industrial Analysis. The chemical composition of the tested cast steel is shown in Table 1. The cast Y-type test ingot (with dimensions: 180x180x60 mm) was subjected to heat treatment (which included solution treatment from 1100°C / water cooling (sample designation H1). Samples with dimensions of 20x25x10 mm were cut from the surface located 10 mm from the bottom surface of the ingot. Then, it was cut into parts using a Labotom-5 cutter from Struers. Parts of the ingot were subjected to isothermal holding at temperatures of 250 (sample designation H2), 400 (sample designation H4), and 600°C (sample designation H6) for 100 hours / air cooling.

The thermodynamic modelling was performed using ThermoCalc software (Version 2019a) with the TCFE7 database.

The samples for the metallographic tests were etched in a 3% solution of HNO₃ acid and ethyl alcohol. Observations of the microstructures of the samples in the states after solution treatment and after isothermal holding were carried out using a Leica MEF 4M light microscope at magnifications of 100 and 500x along with two scanning microscopes: a JEOL JSM 7100 F with an EDS detector from Oxford Instruments, and a Mira Tescan with an Ultim Max EDS detector from Oxford Instruments. The microstructure observations on the scanning microscope were carried out at magnifications within a range of 100–20,000x.

The surface fraction of pearlite in the microstructure of the cast steel sample marked “H6” was determined using a LeicaQWin automatic image analyser cooperating with the Leica MEF 4M light microscope. Measurements were performed on the microstructure images at a 200x magnification. The pearlite dispersion was measured on randomly selected SEM images that

were obtained at a 7,500x magnification. On each of the images, five measuring segments with a length that corresponded to 5 μm in reality were marked. The measurements were performed in accordance with the methodology that is presented in the literature [26]. Hardness tests were carried out via the Vickers method using a Nexus 4000 hardness tester by Innovatest using loads of 10 and 0.1 N (HV₁₀ and HV_{0.1}) [28]. For each sample / phase, five hardness measurements were made.

An abrasive wear resistance test was carried out at room temperature (25 ± 1°C) under the conditions of technically dry friction in the system sample (tested cast steel) – the counter-sample (a ZrO₂ ball with a diameter of 3 mm). The tests were carried out on an Elbit tribotester using the ball-on-disc method. The following parameters were used during the test: load – 5 N; distance – 1000 m; diameter of wear mark – 5 mm; and test duration – 10,000 s [29]. Figure 1 shows the friction node.

Analyses of the wear areas were carried out after the ball-on-disc tests using the microscopes that were previously used to observe the microstructure along with a LEXT™ OLS5100 3D laser confocal microscope by OLYMPUS, which was equipped with specialised LEXT software for image analysis. The confocal microscope made it possible to carry out measurements and record images of the examined surfaces in two modes: microscopic, and confocal (with the use of a 20x objective). This microscope used a beam of light from the visible spectrum with a wavelength of λ = 405 nm.

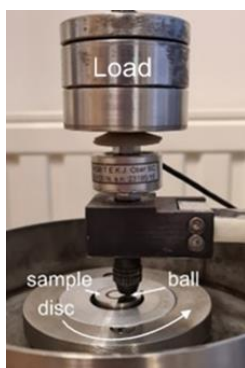


Fig. 1. Friction pair

3. Results and Discussion

3.1. Thermodynamic predictions of phases equilibrium fractions

The influence of the chemical composition of the tested cast steel on the phase-separation process was calculated via the

Table 1.

Chemical compositions of tested GX120MnCr13 cast steel

Data source	Element content, wt. %							
	C	Mn	Si	P	S	Cr	Al	Ti
Standard UN	1.05	11.00	0.30	≤ 0.060	≤ 0.045	1.50	-	-
1.3410 [27]	1.35	14.00	0.90			2.50		
Melt	1.00	14.58	0.60	0.059	0.003	1.67	0.002	0.05

ThermoCalc program using the equilibrium model. The obtained results are shown in Figure 2. On their basis, it was found that cementite and/or ferrite were present within a temperature range of 570–920°C. At the isothermal holding temperatures that were adopted for the tests, pearlite may, thus, occur in the microstructure of the tested cast steel only after an isothermal holding around or under 600°C. According to [10, 11], the pearlitic reaction in high-manganese steel proceeds relatively quickly and increasing the C content from 0.80 to 1.00% accelerates the reaction six-fold. With a C content of 1%, three phases coexist in the alloy: austenite, cementite, and ferrite (stable within a range of 490–625°C). The cementite that occurs within this temperature range is strongly enriched in Mn [11].

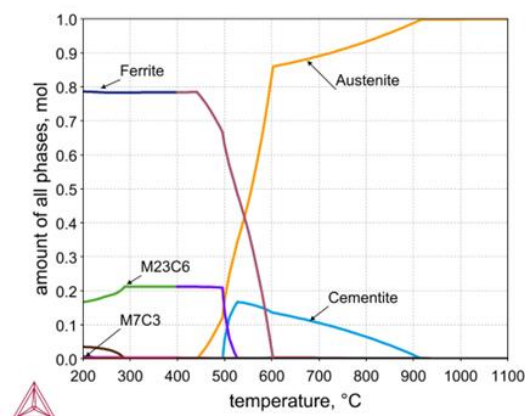


Fig. 2. Participation of phases during cooling of tested cast steel within temperature range of 200–1100°C: FCC – austenite; BCC – ferrite, cementite M₂₃C₆ and M₇C₃ carbides

3.2. Microstructure and hardness

The high contents of C (1.00%) and Mn (14.58%) in the tested GX120MnCr13 cast steel caused that, after the solution treatment, it was characterised by a microstructure of stable austenite with non-metallic inclusions (Fig. 3). SEM-EDS studies showed that the average Mn content in the grain boundary areas was 13.40–15.50%, and the Cr content was 1.60–1.70% (Fig. 3b, c). The applied solution treatment did not fully remove the element segregation effect associated with the phenomenon of crystallization of cast materials. After the isothermal holdings for 100 hours at a temperature of 250°C, the presence of Mn and Cr segregation between the grain boundaries and their interiors could also be found in the microstructure. An example of the analysis of the chemical composition of a microarea is shown in Figure 4.

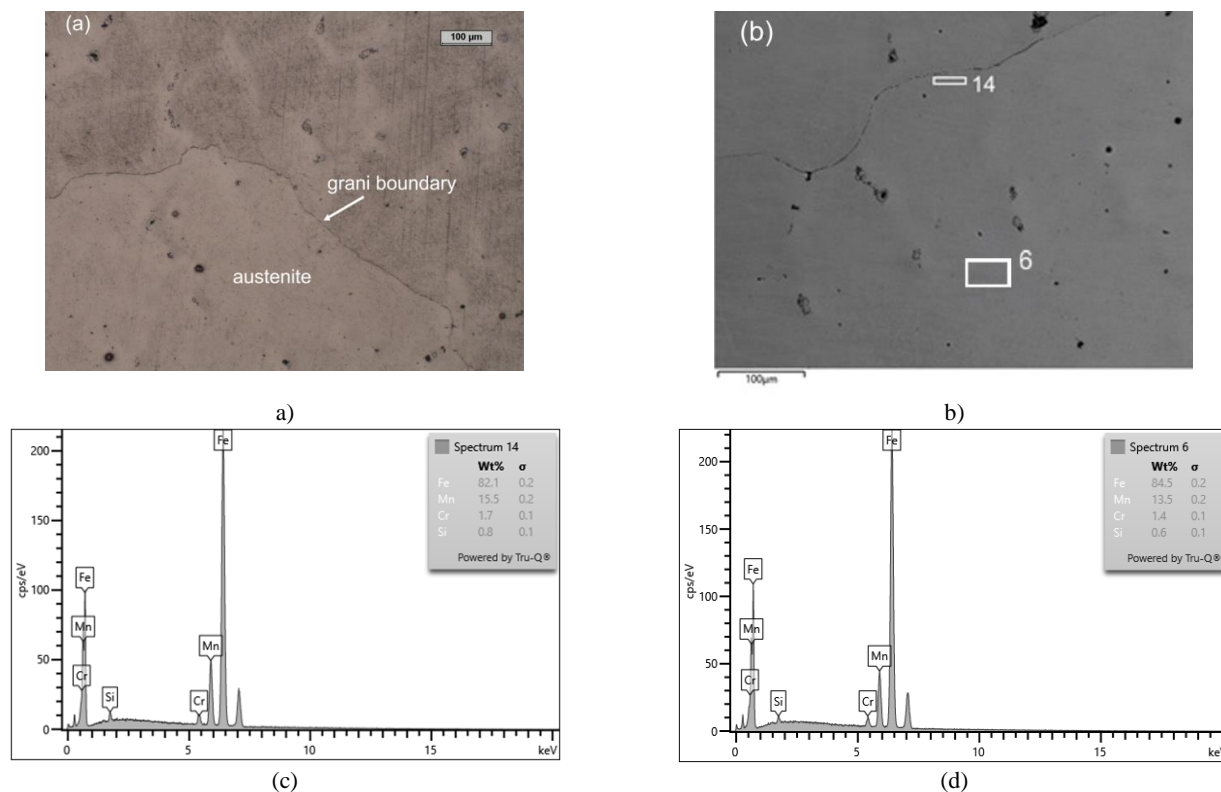


Fig. 3. Example of microstructure of tested cast steel after solution treatment (sample H1) – etching with Nital reagent: (a) light microscope; (b) scanning microscope, analysis of chemical composition from grain boundaries (c) and inside of grain (d) along with X-ray spectrum

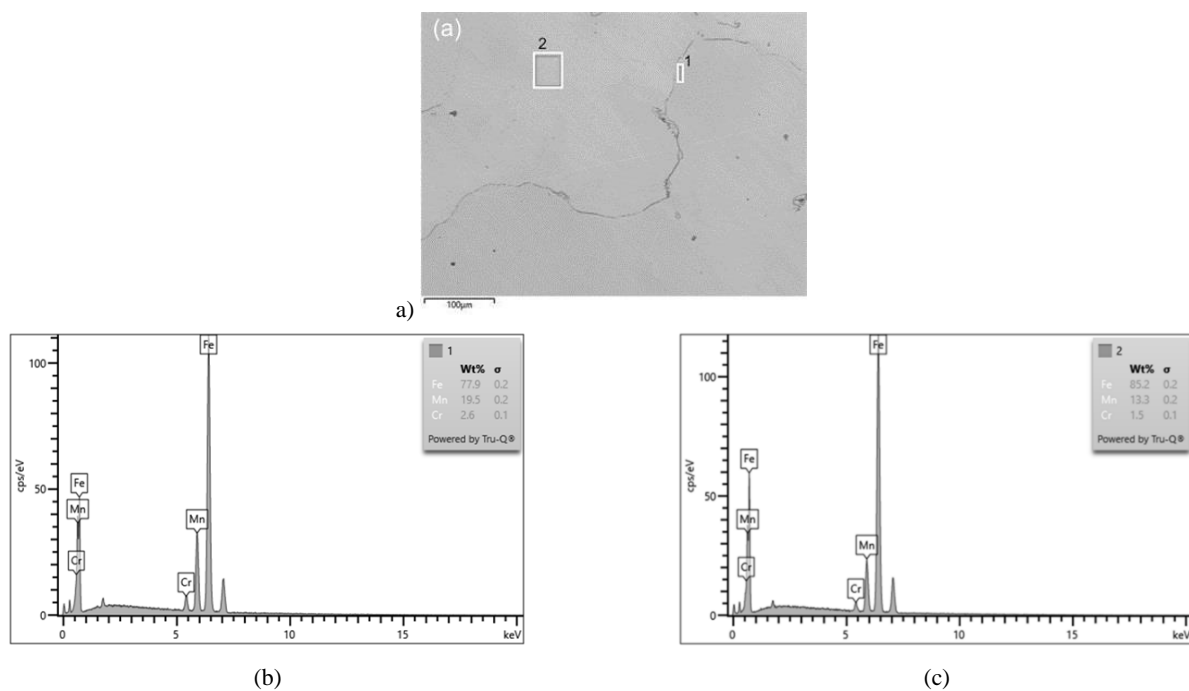


Fig. 4. Example of microstructure (a) and analysis of chemical composition from grain boundaries and inside of grain along with X-ray spectrum (b, c) for cast steel after isothermal holding at 250°C for 100 hours (sample H2) – scanning microscope

In the cast steel isothermal holding at 400°C (sample H4), the segregation of Mn and Cr could also be found between the grain boundary areas and their interiors. The Mn and Cr contents in these areas were comparable to sample H2. The conducted microstructure studies additionally showed the presence of fine precipitates on the grain boundaries (Figs. 5 and 6). The chemical

composition analysis revealed high contents of Mn (28.31–30.04%) and Cr (9.81–11.63%) (Fig. 6). Due to the fact that Mn and Cr are carbide-forming elements, these precipitates were likely complex carbides (Fe, Mn, Cr)₃C that nucleated at the grain boundaries [30].

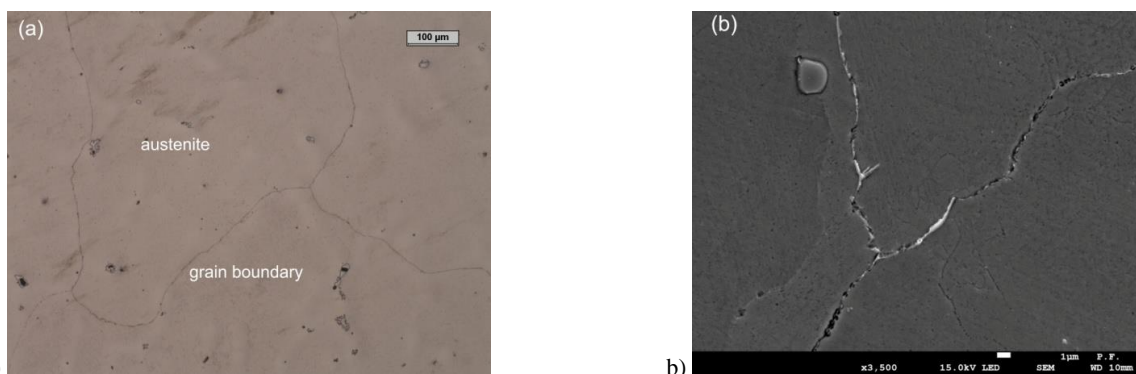


Fig. 5. Microstructure of cast steel after isothermal holding at 400°C for 100 hours (sample H4) – etching with Nital reagent: (a) light microscope (100x magnification); (b) scanning microscope (3500x magnification)

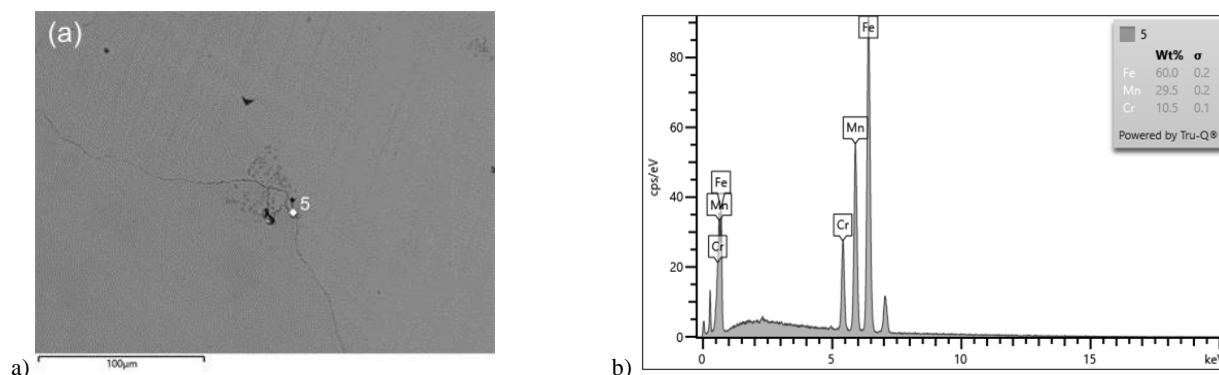


Fig. 6. Example of microstructure (a) and analysis of chemical composition from grain boundaries along with X-ray spectrum (b) for cast steel after isothermal holding at 400°C for 100 hours (sample H4) – scanning microscope

After an isothermal holding at 600°C for 100 hours, the investigated cast steel was characterised by a markedly different microstructure (Figs. 7, 8). The tests showed the presence of numerous islands of lamellar perlite in the microstructure (Fig. 8); the share of this phase was about 41.62%. The obtained microstructures are not directly confirmed in the thermodynamic studies presented in Fig. 2. This is probably related to the research on the cast material, which is characterized by heterogeneity of the structure (segregation of elements) despite the heat treatment. In addition, conducting isothermal holding for 100 hours may have deepened this phenomenon.

The average pearlite dispersion in the tested cast steel was 0.2 μm (the results ranged from 0.148 to 0.297 μm). According to the literature [23], the perlite's dispersion as well as its type [31] can affect a casting's hardness and abrasion resistance [32]. Based on the microhardness tests, the average pearlite hardness was 357.4 HV_{0.1}. The difference between the hardness of the pearlite and the cast steel matrix reached 35 HV_{0.1} (Table 2); which may significantly affect the wear processes of the tested cast steel. The results of the hardness and microhardness measurements of the tested steel are presented in Table 2.

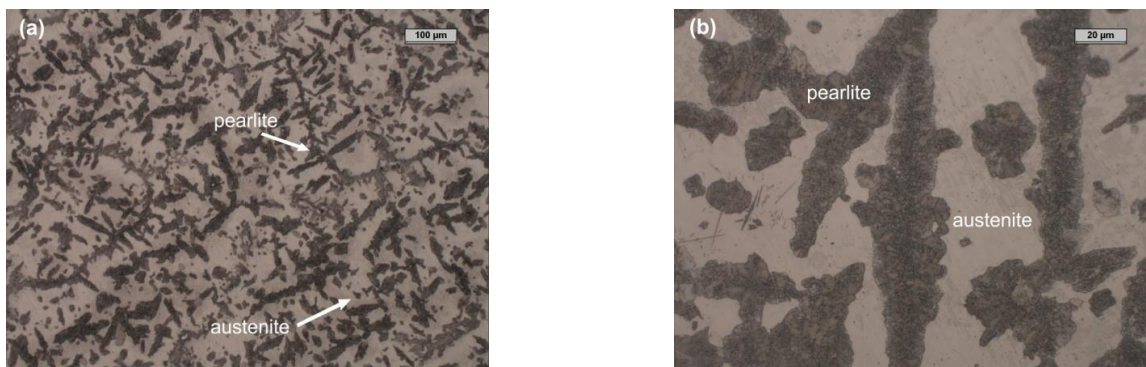


Fig. 7. Microstructure of cast steel after isothermal holding at 600°C for 100 hours (sample H6) – light microscope, etching with Nital reagent: (a) 100x magnification; (b) 500x magnification

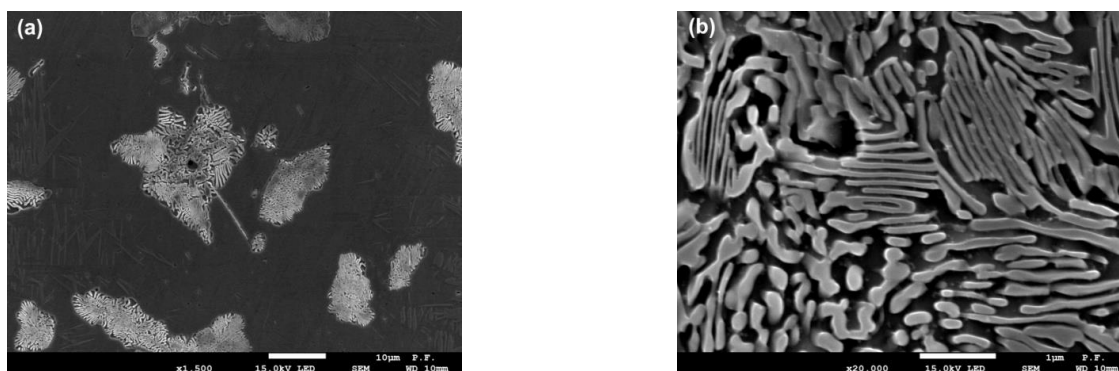


Fig. 8. Microstructure of cast steel after isothermal holding at 600°C for 100 hours (sample H6) – scanning microscope, etching with Nital reagent: (a) 1500x magnification; (b) 20000x magnification

Table 2.

Values of Vickers hardness of tested cast steel (averages of five measurements)

Samples	Hardness HV ₁₀	Standard deviation	Microhardness phases, HV _{0.1} matrix:	Standard deviation
H1 – after solution treatment	221.8	5.19	267.16	4.67
H2 – 250°C / 100 hours	224.2	3.25	258.30	5.11
H4 – 400°C / 100 hours	229.1	3.65	matrix: 256.42	6.61
H6 – 600°C / 100 hours	351.4	6.41	pearlite: 357.40 matrix: 322.60	24.2 8.46

3.3. Test ball on disc

Figure 9 shows the changes in the friction coefficient of the tested materials during the ball-on-disc test, and Table 3 summarizes the results of the tribological tests of the GX120MnCr13 cast steel samples. The initial lapping time for all of the tested materials did not exceed 800s. The coefficient of friction of all of the materials during the initial period of the test had low values (below 0.15 for samples H1, H2, and H6, and 0.25 for sample H4) and then increased rapidly. The friction coefficients that were obtained for the tested samples were unstable and changed during the test; it was only after about 5000–7000s of the test duration that the values of the coefficients stabilised and took on values of approx. 0.4–0.5 (samples H1 and H4), approx. 0.4 (sample H6), and approx. 0.3–0.4 (sample H2). The conducted tests

showed that the coefficient of friction did not depend on the isothermal holding temperature of the tested samples. The lowest average coefficient of friction was obtained for the cast steel that was isothermal holding at 250°C, and the highest could be found in the cast steel that was isothermal holding at 400°C. The coefficients of friction of the starting material and after isothermal holding at 600°C were 0.37 and 0.33, respectively. It should be noted that quite clear fluctuations of the friction coefficient appeared after 5000s in the cases of the materials after isothermal holding at 250° and 400°C (Fig. 9). This is probably due to their lower hardness compared to H6 (austenite - pearlite) and the additional occurrence of microsegregation in the microstructure in the areas of grain boundaries and the presence of manganese cementite precipitates. According to [33], such a phenomenon can be considered to be the initiation of local deformation strengthening on the worn surface.

According to [22, 34], such changes in the friction coefficient were, in turn, caused by the initial formation of abrasive spalling (debris) and their subsequent participation in the rubbing pair. According to [22, 35], loose hard particles that accumulate on a sliding surface contribute to a change in the coefficient of friction and a

simultaneous decrease in mass loss. The reduction of mass losses that was noted in [22] resulted from the fact that the counter sample did not move directly over the material but rather over loose particles that accumulated in the trace of the abrasion.

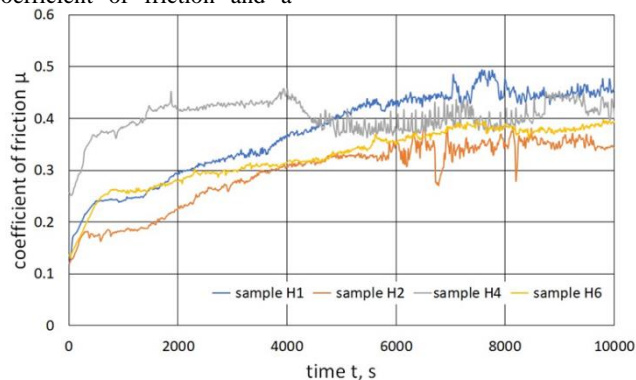


Fig. 9. COF curves of cast steel with testing times

Table 3.

Results for wear rate, and friction coefficient of tested cast steel

Samples	Ball	Wear rate $\cdot 10^{-14}$ $W_s, \text{m}^2/\text{N}$	Friction coefficient μ
H1	ZrO ₂	7.85	0.37
H2		7.59	0.29
H4	1150HV	7.08	0.40
H6		4.28	0.33

Based on the research carried out in this article, the authors did not note any significant changes in the masses of the tested samples; this may have been due to the 5 N load that was used in the test. Another factor that may have also affected the wear was the segregation of Mn and Cr that was found by the authors within the grain boundaries of the tested H2 and H4 cast steel samples and the presence of pearlite in H6.

The calculated wear rate of the tested cast steel was controlled by the initial hardness of the samples. The main mechanism of the cast steel deterioration was abrasive wear. Sample H6 (which contained pearlite in its microstructure) was characterised by better wear resistance (likely caused by its presence). The pearlite clearly decreased the rate of wear as compared to the other tested samples (Fig. 10). The wear rate that was obtained for the cast steel with pearlite was $4.28 \cdot 10^{-14} \text{ m}^2/\text{N}$; for all of the other variants of the tested material, this exceeded a value of $7 \cdot 10^{-14} \text{ m}^2/\text{N}$.

In high-manganese cast steels, the wear rate changes depending on the applied load and/or changes in the content of the main elements, i.e. C and Mn [20]. These elements significantly increase the hardness of cast steel, contributing to the increase in wear resistance. In our case, the tests were carried out with a constant load of 5 N and a constant content of C and Mn, while withstanding we influenced the change in the microstructure of the tested cast steel. Based on the obtained test results, we can conclude that the wear rate is also significantly influenced by the microstructure.

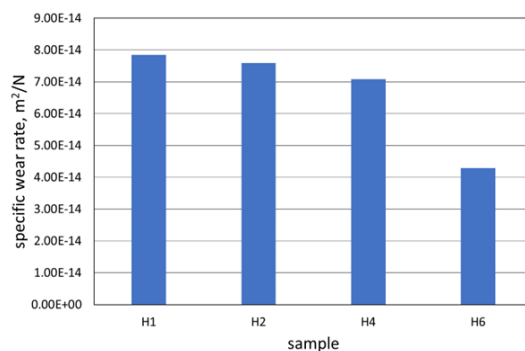


Fig. 10. Specific wear rate of tested cast steel

The analysis of the microstructure of abrasion marks confirmed a lower degree of wear of the cast steel that was isothermal holding at 600°C (Table 3, Figure 11). Figures 11 b, d, f, and h show exemplary profiles of abrasion marks that reflect the degree of the plastic deformation of the tested material. These profiles consisted of distinctive areas: one below the reference line, and two above it. The first one determined the wear depth of the wear mark, while the other two characteristic bulges on either side corresponded to the plastic deformation of the tested material. For sample H6, the bulges at the edges of the wear mark became marginal as compared to the other samples (Fig. 11h). The quantitative characteristics of the abrasion trace profiles are presented in Table 4. The calculated average sizes of the areas below the reference lines for samples H1, H2 and H4 were similar (amounting to 12,558.4, 12,150.5, and 11,336.2 μm^2 , respectively), while the sample H6 area was close to half the size (amounting to 6850 μm^2). Similar changes also applied to the volumes and widths of the obtained abrasion marks (Table 4). It was found that, in the middle part of the wear trace, the depths and widths of the plastic deformation areas depended on the hardness of the sample. Analysing the obtained results, one cannot ignore the possibility of the formation of adhesive bonds between the loss pair. Their breaking led to the tearing of the fragments of one material of the friction pair by the other (which can be seen in Figures 12-14, and 15a).

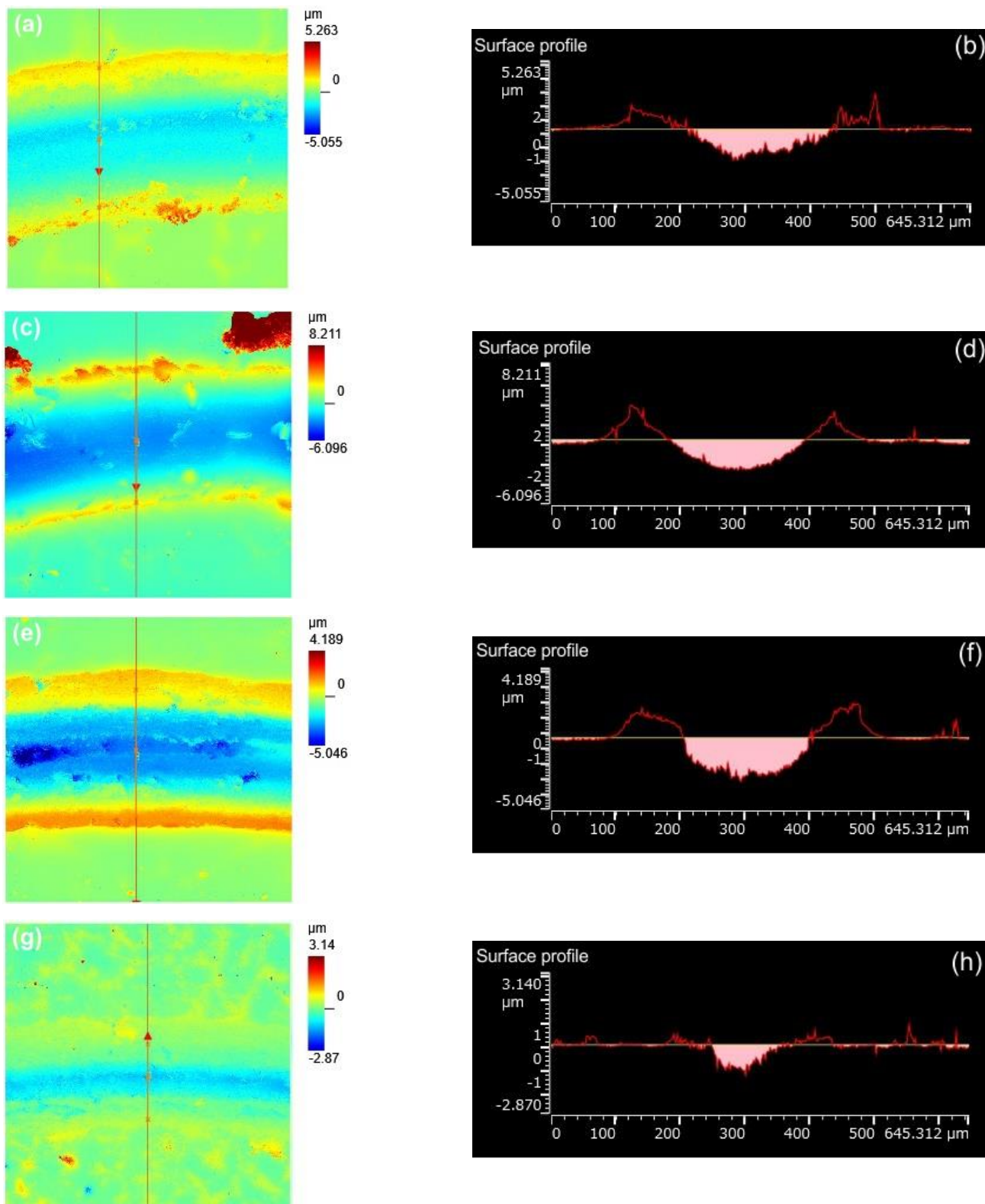


Fig. 11. Topography of surfaces of 2D cast steel and surface profiles on cross-section: (a,b) sample H1; (c,d) sample H2; (e,f) sample H4; (g,h) sample H6

Table 4.

Quantitative characterisation of abrasion profiles that were obtained on tested materials

Samples	Volume, μm^3	Surface area, μm^2	Width of abrasion marks, μm
H1	16,646.6	12,558.4	374.4
H2	20,360.0	12,150.5	295.4
H4	17,645.4	11,336.2	336.6
H6	4,584.1	6,850.3	280.1

*volumes and surface areas – averages of 4 measurements; widths of abrasion marks – averages of 20 measurements (four places on track times five measurements)

3.4. SEM microstructure of wear surface

The complexity of the processes that occur during dry friction result from factors that are related to the abrasive material (e.g. microstructure, hardness, thermal conductivity) as well as the test conditions (e.g. type of counter-sample and load, temperature, time). These make it difficult to unambiguously determine the mechanism of the wear. The local increase in temperature as a result of the dry friction of the tested materials cause that the tribological wear is also accompanied by tribochemical reactions. In the case of the tested material, these were primarily the oxidation processes that occurred between the vapor and the loss. The

presence of oxides on the surfaces of the wipe marks that contained Mn (8.2–9.94%), Cr (1.0–1.2%), and ball-derived Zr (6.2–8.6%) (Fig. 12c, d) may have increased the intensity of the abrasion. This occurred when the oxides did not adhere tightly to the surfaces of the wipe marks; they cracked and detached due to the cyclic action of the counter-specimen (Figs. 13, 14a, 15). The detached fragments of the oxide layer could move freely in the spaces between the ball and the tested cast steels. In addition, the matrix of the tested material was exposed locally; this was confirmed by the analyses of the chemical composition of SEM-EDS (Fig. 13d). This was clearly visible on the wear trace of sample H2, while fewer places could be observed on the traces of samples H4 and H6 (Figs. 13–15) [20].

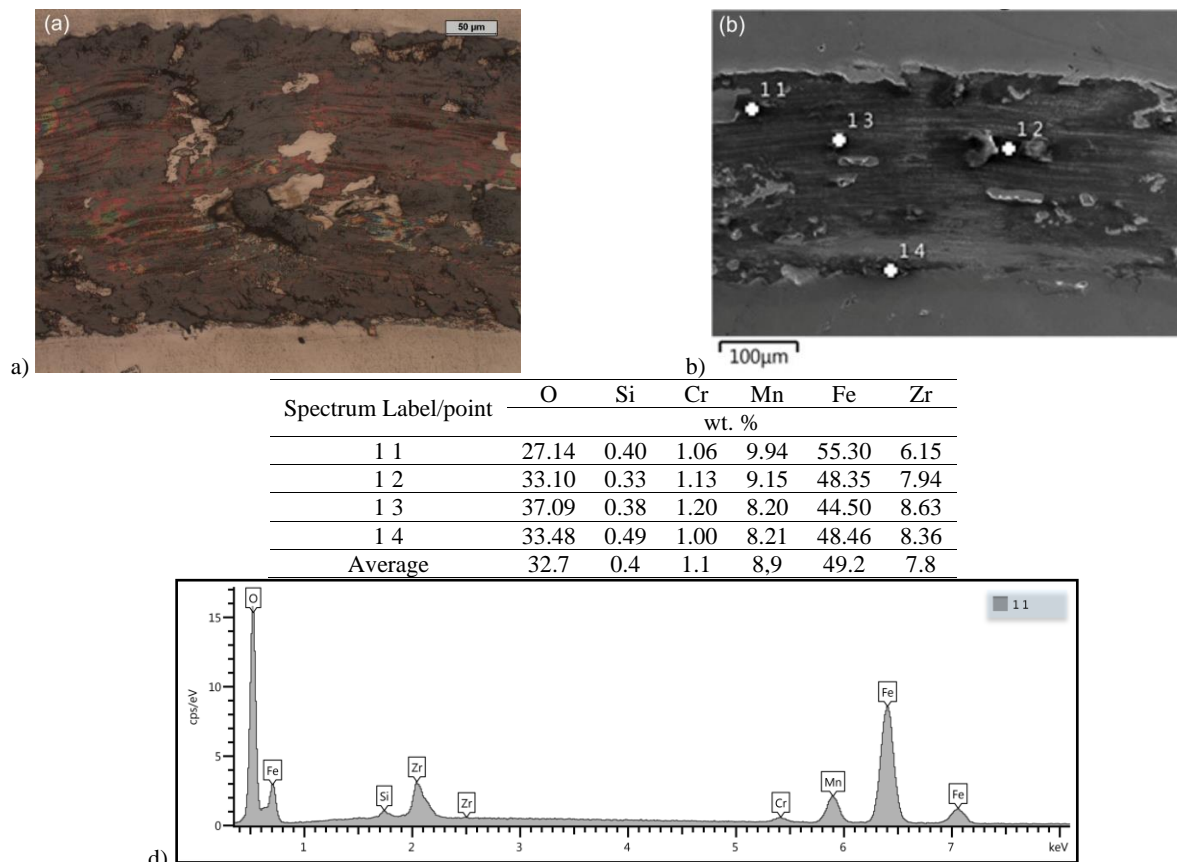


Fig. 12. Wear surfaces with analysis of chemical composition of areas on traces of abrasion (sample H2): (a) light microscope; (b) scanning microscope; (c) spot analysis (scanning microscope); (d) X-ray spectrum from wipe trace (scanning microscope)

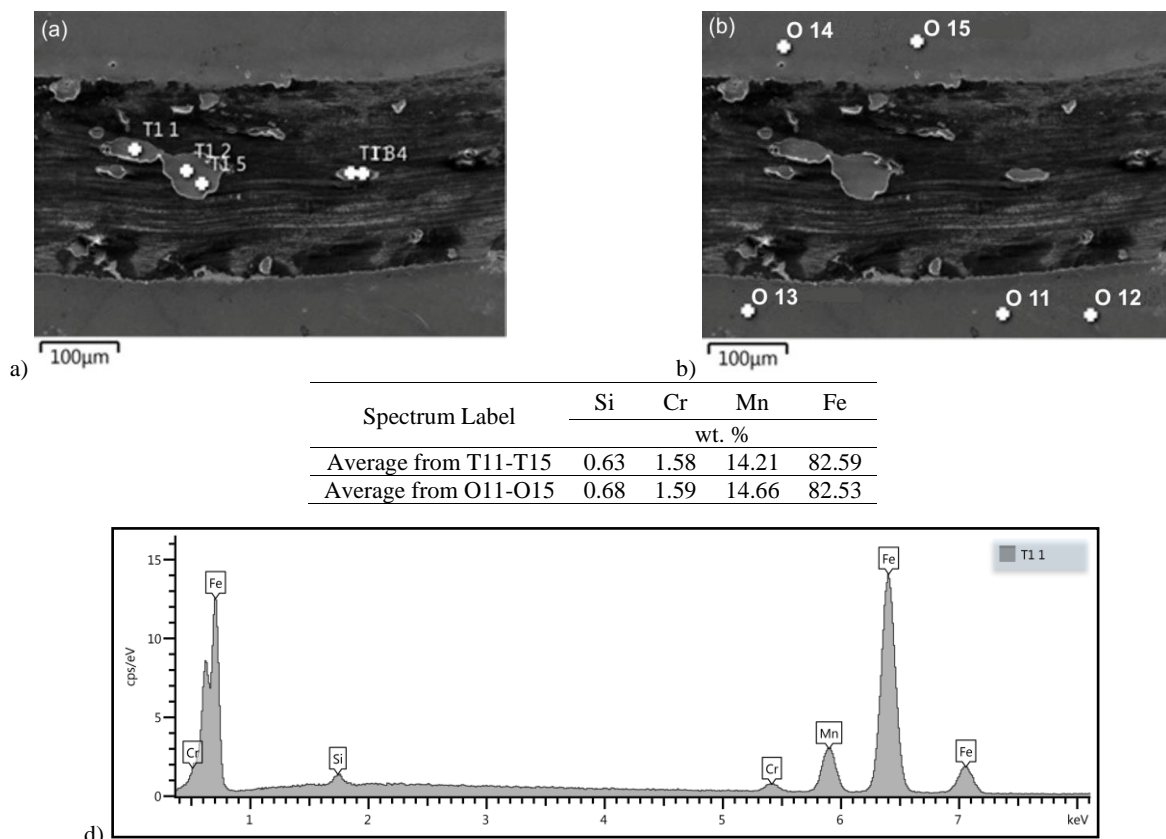


Fig. 13. Wear surfaces with analysis of chemical composition of areas on traces of abrasion (sample H2): (a,b) scanning microscope; (c) mean of point analysis (scanning microscope); (d) X-ray spectrum from wipe trace (scanning microscope)

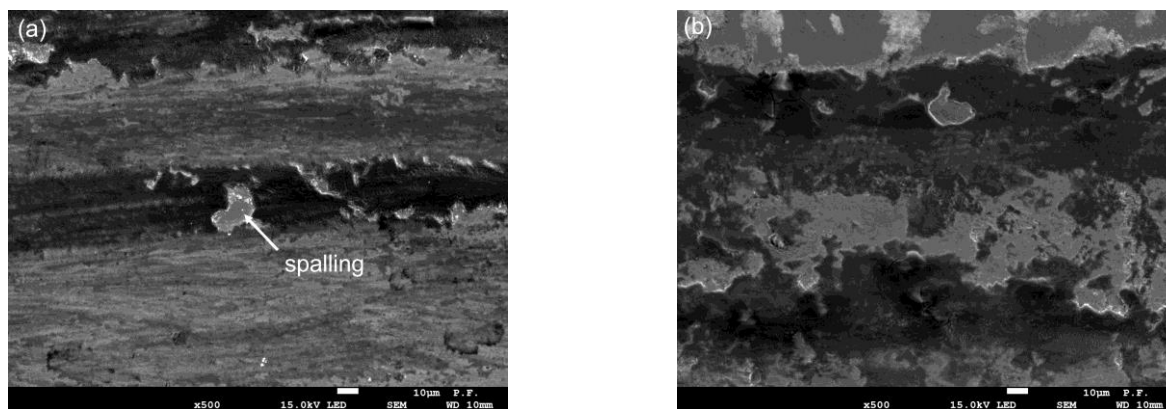


Fig. 14. Wear surfaces with spalling pattern – scanning microscope (500x magnification): (a) sample H4; (b) sample H6

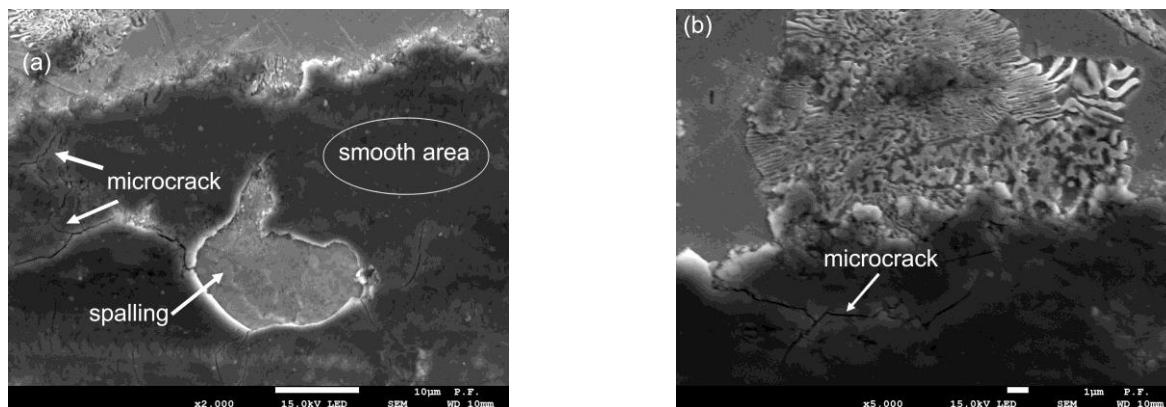


Fig. 15. Wear surfaces with spalling pattern (sample H6) – scanning microscope: (a) 2000x magnification; (b) 5000x magnification

4. Conclusions

The process of the isothermal holding of GX120MnCr13 cast steel at 250 and 400°C for 100 hours not significantly affected its microstructure. In both cases, enrichments of Mn and Cr in the grain boundaries could be found when compared to their interiors. And in the case of the sample that was held at 400°C, precipitates that were enriched in Mn and Cr were additionally found on the grain boundaries.

After heating the tested cast steel at 600°C, it was found that the islands of lamellar pearlite were evenly distributed throughout the microstructure (their share was 41.6%). The pearlite microhardness was 357.4 HV_{0.1}; this resulted in an increase from 221 HV₁₀ (after solution treatment) to 351.4 HV₁₀ (after heating at 600°C) in the hardness of the tested cast steel.

An analysis of the results of the ball-on-disc test showed that both the volume and the surfaces area that was obtained for the cast steel that contained evenly distributed islands of pearlite in the matrix were the smallest (4584.1 µm³ 6850.3 µm², respectively) when compared to the other samples. For the cast steel after solution treatment, these values were 16,646.6 µm³ and 12,558.4 µm², respectively. For the cast steel with the pearlite in the matrix, a reduction in the width of the wear trace could also be found.

The conducted observations of the abrasion marks showed that the dominant phenomena that occurred between the tested rubbing pair were the cracking, detachment, and displacement of the tested material as a result of the cyclical impact of the counter-sample (ZrO₂ ball).

References

- [1] Głównia, J. (2002). *Alloy steel castings – application*. Kraków: FotoBit. (in Polish).
- [2] Maratray, F. (1995). *High carbon manganese austenitic steels*. Paris: International Manganese Institute.
- [3] Krawczyk, J., Matusiewicz, P., Frocisz, Ł., Augustyn-Nadzieja, J., Parzycha, S. (2018). The wear mechanism of mill beaters for coal grinding made-up from high manganese cast. In the 73 WFC, 23-27 September 2018. Kraków, Poland.
- [4] Zambrano, O.A., Tressia, G. & Souza, R.M. (2020). Failure analysis of a crossing rail made of Hadfield steel after severe plastic deformation induced by wheel-rail interaction. *Engineering Failure Analysis*. 115, 1-24. DOI: 10.1016/j.engfailanal.2020.104621.
- [5] Wróbel, T., Bartocha, D., Jezierski, J.; Kalandyk, B., Sobula, S., Tęcza, G., Kostrzewska, K., Feliks, E. (2023). High-manganese alloy cast steel in applications for cast elements of railway infrastructure. In the Proceedings of XXIX International Scientific Conference of Polish, Czech and Slovak Foundrymen Współpraca / Spółpraca, 26-28 April 2023. Niepołomice, Poland.
- [6] Machado, P.C., Pereira, J.I. & Sinatora, A. (2021). Subsurface microstructural dynamic recrystallization in multiscale abrasive wear. *Wear*. 486-487, 204111, 1-14. DOI: 10.1016/j.wear.2021.204111.
- [7] Tressia, G., Penagos, J.J. & Sinatora, A. (2017). Effect of abrasive particle size on slurry abrasion resistance of austenitic and martensitic steels. *Wear*. 376-377, 63-69. DOI: 10.1016/j.wear.2017.01.073.
- [8] Olawale, J.O., Ibitoye, S.A., Shittu, M.D. & Popoola, A.P.I. (2011). A study of premature failure of crusher jaws. *Journal of Failure Analysis and Prevention*. 11(6), 705-709. DOI: 10.1007/s11668-011-9511-7.
- [9] Stradomski Z., Stachura S., Stradomski G. (2013). Fracture mechanisms in steel castings. *Archives of Foundry Engineering*. 13, 88-91. DOI: 10.2478/afe-2013-0066.
- [10] Martin, M., Raposo, M., Prat, O., Giordana, M.F. & Malarria, J. (2017). Pearlite development in commercial Hadfield steel by means of isothermal reactions. *Metallography, Microstructure, and Analysis*. 6, 591-597.
- [11] Martin, M., Raposo, M., Druker, A., Sobrero, C. & Malarria, J. (2016). Influence of pearlite formation on the ductility response of commercial Hadfield steel. *Metallography, Microstructure, and Analysis*. 5(6), 505-511. <https://doi.org/10.1007/s13632-016-0316-7>.
- [12] Tęcza, G. & Sobula, S. (2014). Effect of heat treatment on change microstructure of cast high-manganese Hadfield steel with elevated chromium content. *Archives of Foundry Engineering*. 14, 67-70.
- [13] Krawczyk, J., Bembenek, M. & Pawlik, J. (2021). The role of chemical composition of high-manganese cast steels on

- wear of excavating chain in railway shoulder bed ballast cleaning machine. *Materials*. 16, 1-16. DOI: 10.3390/ma14247794.
- [14] Fedorko, G., Molnár, V., Pribulová, A., Futaš, P., Baricová, D. (2011). The influence of Ni and Cr-content on mechanical properties of Hadfield's steel. In the 20th Anniversary International Conference on Metallurgy and Materials – Metal, May 2011 (pp. 18-20). Brno, Czech Republic.
- [15] Najafabadi, V., Amini, K. & Alamdarlo, M. (2014). Investigating the effect of titanium addition on the wear resistance of Hadfield steel. *Metallurgical Research and Technology*. 111(6), 375-382. DOI: 10.1051/metal/2014044.
- [16] Tęcza, G. & Garbacz-Klempka, A. (2016). Microstructure of cast high-manganese steel containing titanium. *Archives of Foundry Engineering*. 16(4), 163-168. DOI: 10.1515/afe-2016-0103.
- [17] Kalandyk, B., Tęcza, G., Zapala, R. & Sobula S. (2015). Cast high-manganese steel – the effect of microstructure on abrasive wear behaviour in Miller test. *Archives of Foundry Engineering*. 15, 35-38. DOI: 10.1515/afe-2015-0033.
- [18] Shan, Q., Ge, R., Li Z., Zhou, Z., Jiang, Y., Lee, Y.-S. & Wu, H. (2021). Wear properties of high-manganese steel strengthened with nano-sized V₂C precipitates. *Wear*. 482-483, 203922, 1-10. DOI: 10.1016/j.wear.2021.203922.
- [19] Ayadi, S. & Hadji, A. (2021). Effect of chemical composition and heat treatments on the microstructure and wear behavior of manganese steel. *International Journal of Metalcasting*. 15(2), 510-519. DOI: 10.1007/s40962-020-00479-2.
- [20] Gürol, U. & Can Kurnaz, S. (2020). Effect of carbon and manganese content on the microstructure and mechanical properties of high manganese austenitic steel. *Journal of Mining and Metallurgy Section B - Metallurgy*. 56, 171-182. DOI: 10.2298/JMMB191111009G.
- [21] Kalandyk, B., Zapala, R., Kasińska, J. & Madej, M. (2021) Evaluation of microstructure and tribological properties of GX120Mn13 and GX120MnCr18-2 cast steels. *Archives of Foundry Engineering*. 21(3), 67-76. DOI: 10.24425/afe.2021.138681.
- [22] Atabaki, M.M., Lafaril, S. & Abdollah-Pour, H. (2012) Abrasive wear behavior of high chromium cast iron and Hadfield steel-A comparison. *Journal of Iron and Steel Research, International*. 19, 43-50. DOI: 10.1016/S1006-706X(12)60086-7.
- [23] Gierek, A. (2005). *Zużycie tribologiczne*. Gliwice: Wyd. Politechniki Śląskiej.
- [24] Kalandyk, B., Zapala, R., Madej, M., Kasińska, J. & Piotrowska, K. (2022). Influence of pre-hardened GX120Mn13 cast steel on the tribological properties under technically dry friction. *Tribologia*. 3, 17-24. DOI: 10.5604/01.3001.0016.1020.
- [25] El-Fawkhry, M.K., Fathy, A.M., Eissa, M.M. & El-Faramway, H. (2014). Eliminating heat treatment of Hadfield steel in stress abrasion wear applications, *International Journal of Metalcasting*. 8, 29-36. DOI: 10.1007/BF03355569.
- [26] Cybo, J., Jura, S. (1995). *Functional description of isometric structures in quantitative metallography. Functional description of isometric structures in quantitative metallography*. Gliwice: Wyd. Politechniki Śląskiej. (in Polish).
- [27] Standard EN 10349: 2009. Cast steel castings - Castings made of manganese austenitic cast steel. (in Polish).
- [28] Standards PN-EN ISO 6507-1: 2007. Metallic materials - Vickers hardness test.
- [29] Standards ISO 20808: 2016. Fine ceramics (advanced ceramics, advanced technical ceramics) - Determination of friction and wear characteristics of monolithic ceramics by ball-on-disc method.
- [30] Mishra, S. & Dalai R. (2021). A comparative study on the different heat-treatment techniques applied to high manganese steel. *Materials Today: Proceedings*. 44(1), 2517-2520. DOI: 10.1016/j.matpr.2020.12.602.
- [31] Kawalec, M. & Fraś, E. (2009). Effect of silicon on the structure and mechanical properties of high-vanadium cast iron. *Archives of Foundry Engineering*. 9(3), 231-234.
- [32] Dziubek, M., Rutkowska-Gorczyca, M., Dudziński, W. & Grygier, D. (2022). Investigation into changes of microstructure and abrasive wear resistance occurring in high manganese steel X120Mn12 during isothermal annealing and re-austenitisation process. *Materials*. 15(7), 2622. DOI: 10.3390/ma15072622.
- [33] El Fawkhry M. K. (2021). Modified Hadfield steel for castings of high and low gouging applications. *International Journal of Metalcasting*. 15(4), 613-624. DOI: 10.1007/s40962-020-00492-5.
- [34] Lindroos, M., Apostol, M., Heino, V., Valtonen, K., Laukkanen, A., Holmberg, K. & Kuokkala, V.T. (2015). The deformation, strain hardening, and wear behavior of chromium-alloyed Hadfield steel in abrasive and impact conditions. *Tribology Letters*. 57, 1-11. DOI: 10.1007/s11249-015-0477-6.
- [35] Luo, Q. & Zhu, J. (2022). Wear property and wear mechanisms of high-manganese austenitic Hadfield steel in dry reciprocal sliding. *Lubricants*. 10(3), 1-18. DOI: /10.3390/lubricants10030037.